Phenomenology of quantum eigenstates in mixed-type systems: Lemon billiards with complex phase space structure

Črt Lozej,[1,2] Dragan Lukman,[1] and Marko Robnik[1]

[1]*CAMTP - Center for Applied Mathematics and Theoretical Physics, University of Maribor, Mladinska 3, SI-2000 Maribor, Slovenia*

[2]*Max Planck Institute for the Physics of Complex Systems, Nöthnitzer Strasse 38, D-01187 Dresden, Germany*

(Received 18 July 2022; accepted 20 October 2022; published 7 November 2022)

The boundary of the lemon billiards is defined by the intersection of two circles of equal unit radius with the distance $2B$ between their centers, as introduced by Heller and Tomsovic [E. J. Heller and S. Tomsovic, Phys. Today **46**, 38 (1993)]. This paper is a continuation of our recent papers on a classical and quantum ergodic lemon billiard ($B = 0.5$) with strong stickiness effects [Č. Lozej *et al.*, Phys. Rev. E **103**, 012204 (2021)], as well as on the three billiards with a simple mixed-type phase space and no stickiness [Č. Lozej *et al.*, Nonlin. Phenom. Complex Syst. **24**, 1 (2021)]. Here we study two classical and quantum lemon billiards, for the cases $B = 0.1953,\ 0.083$, which are mixed-type billiards with a complex structure of phase space, without significant stickiness regions. A preliminary study of their spectra was published recently [Č. Lozej, D. Lukman, and M. Robnik, Physics **3**, 888 (2021)]. We calculate a very large number (10^6) of consecutive eigenstates and their Poincaré-Husimi (PH) functions, and analyze their localization properties by studying the entropy localization measure and the normalized inverse participation ratio. We introduce an overlap index, which measures the degree of the overlap of PH functions with classically regular and chaotic regions. We observe the existence of regular states associated with invariant tori and chaotic states associated with the classically chaotic regions, and also the mixed-type states. We show that in accordance with the Berry-Robnik picture and the principle of uniform semiclassical condensation of PH functions, the relative fraction of mixed-type states decreases as a power law with increasing energy, thus, in the strict semiclassical limit, leaving only purely regular and chaotic states. Our approach offers a general phenomenological overview of the structural and localization properties of PH functions in quantum mixed-type Hamiltonian systems.

DOI: 10.1103/PhysRevE.106.054203

I. INTRODUCTION

Classical generic Hamiltonian systems exhibit both regular and chaotic motion [1], depending on the initial condition. They are referred to as systems with divided phase space or mixed-type systems because the phase space is divided into regular and chaotic invariant components, with an intricate hierarchical structure of islands of stability embedded in the chaotic sea. Accordingly, the chaotic sea(s) and islands of stability, comprised of invariant tori, may be combined into disjoint measurable subsets with a positive a Liouville measure (phase space volume). According to the correspondence principle, one expects that the eigenstates of the equivalent quantized system should behave similarly. The states may be separated into subsets that correspond to either the chaotic or regular classical dynamics, with a spectral density that is equal to the classical Liouville measure of the corresponding invariant component in the phase space. The idea was first conjectured by Percival [2], further elaborated by Berry [3,4], and later developed into the principle of uniform semiclassical condensation (PUSC); see [5] and references therein. The states may be separated, depending on the overlap with either the regular or chaotic part of the classical phase space, by means of Wigner functions or Husimi functions. Following PUSC, the high-lying eigenstates are supported either on the chaotic sea or the invariant tori forming the islands of stability in the ultimate semiclassical limit. The partial spectrum of the regular states follows Poissonian statistics, while the spectral statistics of the chaotic states are well described by random matrix theory (RMT) [6,7]. The whole spectrum may be collectively described by the Berry-Robnik spectral statistics [8]. An abundance of numerical evidence corroborates the Berry-Robnik picture and PUSC as its foundation [9–18]. However, a true separation to regular and chaotic states may only be expected in the asymptotic semiclassical limit (where the action is large compared to $\hbar$). Before reaching this asymptotic regime, many states will exhibit a mixed behavior with various tunneling processes between the structures of the classical phase space, and much less is known about this regime despite its rich and interesting phenomenology. For instance, the mixed eigenstates support important physical phenomena, such as chaos-assisted tunneling [19], that has recently been shown to have useful applications in quantum simulation [20]. For a general introduction and a rather complete

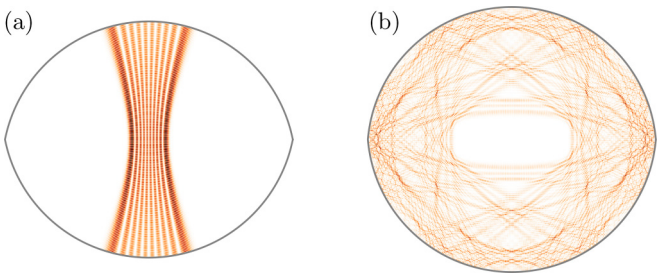

FIG. 1. Illustration of the two lemon billiards considered in this work together with the probability distributions of a high-lying quantum eigenstate. (a) $B = 0.1953$, regular eigenstate at $k = 462.122$; (b) $B = 0.083$, chaotic eigenstate at $k = 457.533$.

account of quantum chaos, we refer to the books by Stöckmann [6] and Haake [7], and to the recent review papers on the stationary quantum chaos in generic (mixed-type) systems [21,22].

In this paper, we compute and study the properties of a large number (approximately 10^6) of eigenstates for two examples of lemon billiards with complex divided phase spaces. Billiards are excellent examples of generic model Hamiltonian systems, widely used for studies in quantum chaos. The lemon billiards were introduced by Heller and Tomsovic [23] and have been extensively studied (including some generalizations) [24–31] in the context of classical regular and chaotic dynamics, and as quantum billiards, including our recent works [32–34].

The lemon billiard table is defined as the intersection of two circles of equal unit radius, with a distance of $2B$ between their centers (the construction is explained in Appendix A). In this work, we study classical and quantum mechanics of two lemon billiards, namely, $B = 0.1953$ and $B = 0.083$. They are illustrated in Fig. 1. It must be emphasized that although the lemon billiards all belong to the same family as for the mathematical definition, individually they have quite different and very rich dynamical properties, which makes them important in both the classical and quantum contexts. The specific parameters were chosen with the following considerations. The phase space of both billiards consists of one significant chaotic component and several islands of stability. In the $B = 0.1953$ case, three major island chains are present, while $B = 0.083$ shows a complex web of many island chains. In both cases, stickiness effects (see Refs. [35,36] for an introduction to the phenomenon) are negligible. This fact is of great significance since classical stickiness also has considerable effects on the quantum dynamics and structure of the eigenstates, as we have recently shown for the case of the presumably ergodic $B = 0.5$ billiard in Ref. [32]. Previously, we have also studied the aspects of quantum chaos in three mixed-type lemon billiards, $B = 0.42,\ 0.55,\ 0.6$, with a simple structure (only one dominant chaotic component without stickiness regions, coexisting with only one large regular component), in Ref. [33]. The cases considered in the present paper allow for an increased complexity and richness of the mixed eigenstates and tunneling effects, but still exclude the effects of strong partial transport barriers that would classically result in stickiness. The discovery of these dynamically different and interesting lemon billiards has only been made possible thanks to the recent extensive analysis of Lozej [30]. The entire family of classical lemon billiards for a dense set of about 4000 values of $B \in [0.01, 0.99\,975]$ (in steps of $dB = 0.00\,025$) has been systematically analyzed for their phase space structure and stickiness effects.

A study of quantum energy spectra of the billiards considered in the current work has recently been published in [34], where specifically we studied the fluctuation of the number of energy levels around the mean value determined by the Weyl rule with the perimeter corrections, and the energy level spacing distributions for all (four) symmetry classes.

The main purpose of the present paper is the phenomenological analysis of the eigenstates of the two selected quantum lemon billiards, $B = 0.1953$ and 0.083, with the following goals: (i) To calculate the *Poincaré-Husimi* (PH) [37,38] functions of the eigenstates, analyze their structure in the phase space in relationship to the classical phase portrait, and examine the quantum localization of chaotic eigenstates in the phase space. (ii) To establish the relationships between various localization and classical-quantum overlap measures in order to present a complete overview of the eigenstates in the PH representation. (iii) To observe the condensation of the eigenstates on classical invariant components, with progressive energy, in the context of the Berry-Robnik picture of quantum chaos in mixed-type systems [8] and the principle of uniform semiclassical condensation [5].

The main results are the following. The great majority of PH functions are found to be well supported either on invariant tori in the regular islands or on the chaotic component, thus obeying the principle of uniform semiclassical condensation of Wigner functions [5]. PH functions of mixed type exist and show a wide variety of tunneling states between different classical structures. The distributions of localization and overlap measures may be used to identify the various interesting regimes and quantify their prevalence. The proportion of mixed-type states shows a power-law decay with increasing energy in both billiards with an overall exponent of $\gamma \approx 0.3$ and a local variation from 0.1 to 0.5 pertaining to different mixed-state regimes.

The paper is organized as follows. In Sec. II, we examine the classical dynamical properties of the two lemon billiards under consideration. In Sec. III, we define the quantum billiard problem, discuss its numerical solution, and introduce the Poincaré-Husimi functions of the eigenstates. In Sec. IV, we introduce the overlap index M and propose how to separate the regular and chaotic eigenstates in the sense of Berry-Robnik [8]. In Sec. V, we introduce and compute the localization measures of the regular, chaotic, and mixed-type eigenstates, study the structure of their probability distributions, and relate it to the Poincaré-Husimi functions of individual eigenstates. In Sec. VI, we study the connection between the overlap index M and the localization measures. In Sec. VII, we analyze the energy dependence of the whole picture. In Sec. VIII, we summarize and discuss the results and present the conclusions. Appendix A gives a short overview of the construction and geometry of the lemon billiards and Appendix B presents some relevant results on stickiness and recurrence time statistics.

II. PHASE SPACE STRUCTURE OF LEMON BILLIARDS

A billiard is a dynamical system which consists of a free moving point particle confined inside a closed domain $\mathcal{B}$ in Euclidean space, referred to as the billiard table. The particle moves freely inside the billiard table in straight lines and is specularly reflected when hitting the edge of the table. The family of lemon billiards is formed by the intersection of two circles of equal unit radius with a distance of $2B$ between their centers, where $B \in (0, 1)$. As usual, we consider the billiard as a discrete dynamical system, taking the boundary as the surface of the section. We use the canonical variables to specify the location q and the momentum component p on the boundary at the collision point, so that the classical phase space is a cylinder $(q, p) \in [0, L] \times (-1, 1)$, where q is the arclength (periodic with a period equal to the circumference of the boundary L) and $p = \sin(\alpha)$ is the sine of the angle of reflection. For more details on construction of the lemon billiards, the canonical variables, and geometric properties, see Appendix A. The bounce map, mapping from collision to the next collision, $(q, p) \to (q', p')$, is area preserving as in all billiard systems [39].

Due to the two kinks (corners at $y = 0$), the Lazutkin invariant tori (related to the boundary glancing orbits) are broken. The period-2 orbit connecting the centers of the two circular arcs is always stable (and therefore surrounded by a regular island), except for the case $B = 1/2$, where it is a marginally unstable orbit. This case is presumably ergodic and has been treated in our recent paper [32]. In all other cases, the phase space is divided (mixed type) with one dominant chaotic sea (that is significantly larger than all other chaotic components) and typically a multitude of islands of stability. Keeping in mind the Berry-Robnik picture, it is useful to compute the relative measure pertaining to chaotic and regular components in the phase space. We compute the relative areas χ_c and $\chi_r = 1 - \chi_c$ on the surface of the section [two-dimensional phase space of canonical coordinates (q, p)] by using the methods presented in Ref. [40]. However, the spectral density of the regular or chaotic states is given by the Liouville measure [volume in the energy surface of the full four-dimensional phase space in Cartesian coordinates (x, p_x, y, p_y)]. To convert the area into the volume, $\chi_c \to \rho_c$, we use a formula due to Meyer [41] given in Appendix A.

The phase portrait for the billiard $B = 0.1953$ is shown in Figs. 2 and 3. The relative fractions of the chaotic component are $\chi_c = 0.3585$ or $\rho_c = 0.2804$ (which is the Berry-Robnik parameter). Three independent regular island chains are clearly visible, the largest one around the period-2 orbit which is densely covered by the invariant tori, with no visible thin chaotic layers inside. We denote the largest island chain by $\mathcal{L}$, the second largest one by $\mathcal{M}$, and the smallest one by $\mathcal{S}$. The relative phase space volume of all three regular regions taken together is $\rho_r = 1 - \rho_c = 0.7196$. The chaotic sea is very uniform, with no significant stickiness regions, as evident in the S plot (introduced in Ref. [30]). The S parameter is the local coefficient of variation of the recurrence times into small areas of the chaotic component. When $S = 1$, the distribution of recurrence times is exponential, as expected for uniform chaos. If $S > 1$, this indicates a modified recurrence time distribution, i.e., stickiness. For more details, see

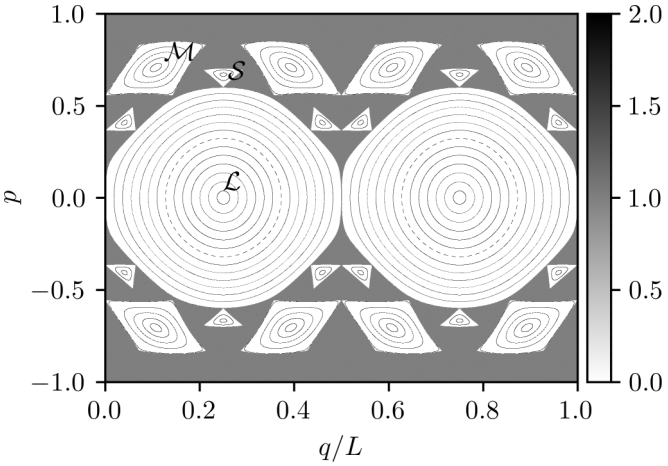

FIG. 2. The phase portrait of the lemon billiard $B = 0.1953$. The chaotic component is mapped by a single chaotic orbit and recurrence time statistics are presented as grayscale plot. The gray coding on the color bar is the quantity S measuring the stickiness in the chaotic component (see Appendix B), showing that we uniformly have $S \approx 1$, and thus no significant stickiness. Inside the islands of stability, we show some representative invariant tori. $\chi_c = 0.3585$, $\rho_c = 0.2804$, $\rho_r = 1 - \rho_c = 0.7196$, and $L = 5.4969$

Appendix B. The phase portrait as shown in Fig. 4 for the billiard $B = 0.083$ is more complex. The relative fraction of the area of the chaotic component of the bounce map is $\chi_c = 0.2168$, while the relative fraction of the phase space volume of the same chaotic component is $\rho_c = 0.1617$. Thus, the relative phase space volume fraction of the complementary regular regions is $\rho_r = 1 - \rho_c = 0.8383$. Also in this case, the chaotic sea is rather uniform, with no significant stickiness regions. The details of the desymmetrized part of the phase space are shown in Fig. 5. We can conclude that the two cases $B = 0.1953,\ 0.083$ are interesting to verify the Berry-Robnik picture of quantum billiards, including the possible quantum localization of the chaotic eigenstates and the universal statistical properties of the localization measures. The two cases add a level of increased complexity for the island structure,

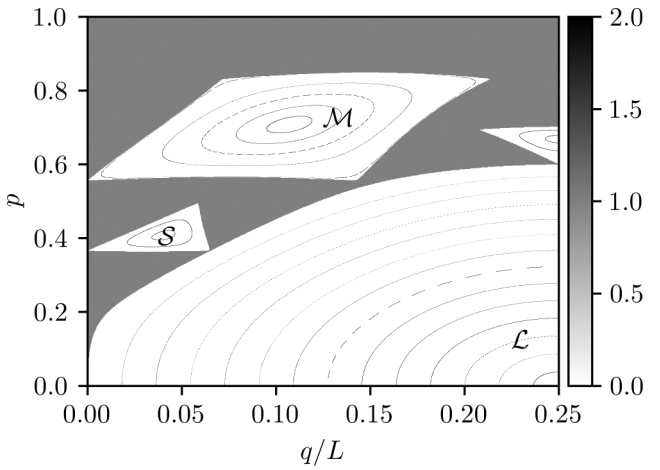

FIG. 3. The details of the desymmetrized part of the phase portrait of the lemon billiard $B = 0.1953$. For a description, see Fig. 2.

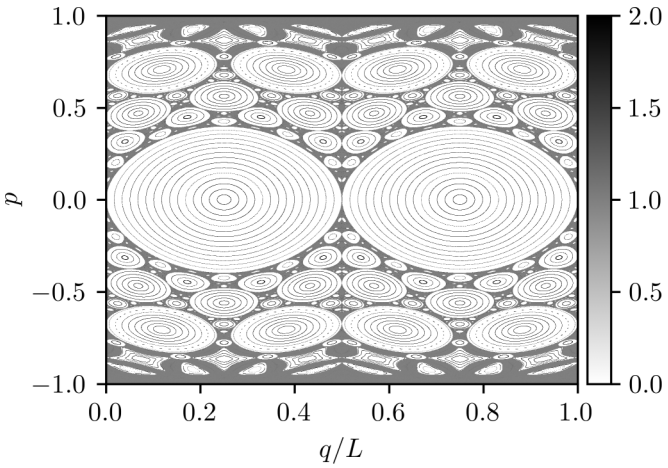

FIG. 4. The phase portrait of the lemon billiard $B = 0.083$. For a description, see Fig. 2. $\chi_c = 0.2168$, $\rho_c = 0.1617$, $\rho_r = 1 - \rho_c = 0.8383$, and $L = 5.9508$.

while keeping the chaotic sea uniform, without stickiness, as in the examples of the previous paper [33] where simple single-island phase spaces were studied. This is quite different from the ergodic case $B = 0.5$ studied in Ref. [32], where the stickiness effects are strongly pronounced and are reflected in the nonuniversal localization properties of quantum (chaotic) eigenstates.

III. THE SCHRÖDINGER EQUATION AND THE POINCARÉ-HUSIMI FUNCTIONS

The quantum billiard $\mathcal{B}$ is described by the stationary Schrödinger equation, in the chosen units ($\hbar^2/2m = 1$), given by the Helmholtz equation

$$\Delta\psi + k^2\psi = 0, \tag{1}$$

with the Dirichlet boundary conditions $\psi|_{\partial\mathcal{B}} = 0$. The energy is $E = k^2$.

The *mean number of energy levels* $\mathcal{N}(E)$ below $E = k^2$ is determined quite accurately, especially at large energies,

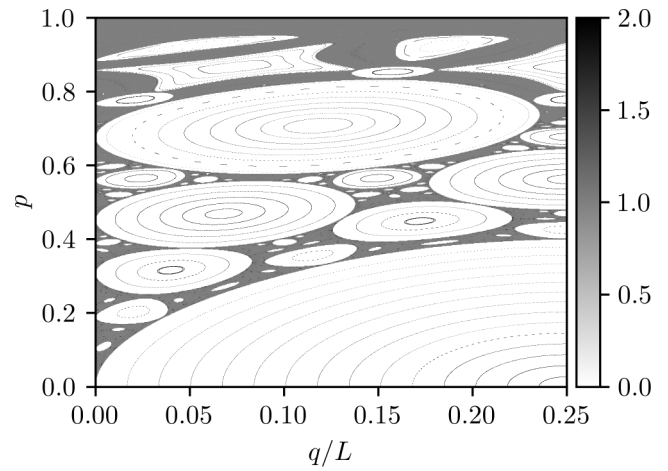

FIG. 5. The details of the desymmetrized part of the phase portrait of the lemon billiard $B = 0.083$. For a description, see Fig. 2.

asymptotically exactly, by the celebrated Weyl formula (with perimeter corrections) using the Dirichlet boundary conditions, namely,

$$\mathcal{N}(E) = \frac{A\,E}{4\pi} - \frac{L\,\sqrt{E}}{4\pi} + c, \tag{2}$$

where c are small constants determined by the corners and the curvature of the billiard boundary. Differentially, they play no role. Thus, the density of states $d(E) = d\mathcal{N}/dE$ is equal to

$$d(E) = \frac{A}{4\pi} - \frac{L}{8\pi\sqrt{E}}. \tag{3}$$

As shown in the previous paper [34] and according to the theoretical predictions by Steiner [42,43], the fluctuations of the number of energy levels (mode fluctuations) around the mean value of Eq. (2) grow with k, such that their variance increases linearly with k in integrable systems and as logarithmically with k in ergodic chaotic systems. For the mixed-type systems, it is something in between, namely, the variance is the sum of the variances of the regular and of the chaotic parts, provided that we can treat them as statistically independent of each other, which in the semiclassical regime is a valid assumption according to the Berry-Robnik picture [8]. Thus, the fluctuations at large values of k in all cases can be very large, and the standard deviation even diverges as $k \to \infty$. In ergodic chaotic systems, the distribution of fluctuations is predicted to be Gaussian [42,43], while in Ref. [34], we have shown that it is almost always Gaussian, or very close to that, even in the integrable and mixed-type systems.

Our numerical method to compute the eigenfunctions is based on the Vergini-Saraceno scaling method [44,45], with two possible basis sets, plane waves or circular waves (Bessel functions for the radial part and trigonometric functions for the angular part). The numerical methods are available as part of a PYTHON numerical library [45,46]. The agreement between calculations using both basis sets is good, so all the presented calculations were done using the plane-wave basis because of the much faster computation. The method computes several eigenstates within a small energy interval per diagonalization, and its efficiency allowed us to compute almost 10^6 eigenstates in the PH representation for each billiard. However, the precision of the computed energy levels decreases with the distance from the center of the energy interval. Thus, even after careful comparison of the levels in overlapping energy intervals, errors in the accumulation of levels still occur and some levels are lost. The number of missing levels was never larger than 1 per 1000 levels and, due to the overall large number of eigenstates, this should have very little effect on the statistical results.

The lemon billiards have two reflection symmetries, thus four symmetry classes: even-even, even-odd, odd-even and odd-odd. For the purpose of our analysis, we have considered only the quarter billiard, i.e., the odd-odd symmetry class. We have calculated the energy spectra and PH functions for each billiard in spectral stretches of about 10^6 states, starting from the 10^4th state. In order to compare the energy-dependent results between the two billiards, we must first exclude the effect of densities of states. We use the standard unfolding

procedure and insert the spectra into the Weyl formula (2),

$$e_n := \mathcal{N}(E_n), \tag{4}$$

where e_n is the unfolded energy of the nth state. This results in a spectrum where the mean level spacing is equal to one.

As in previous works [32–34,47–50], we now define the Poincaré-Husimi (PH) functions, thereby introducing the quantum phase space whose structure should correspond to the classical phase space in the semiclassical limit. Thus, instead of studying the eigenstates by means of the wave functions $\psi_m(\mathbf{r})$ as solutions of the Helmholtz equation (1), we define PH functions as a special case of Husimi functions [51], which are, in turn, Gaussian smoothed Wigner functions [52]. They are very natural for billiards. Following Tuale and Voros [37] and Bäcker *et al.* [38], we define the properly L-periodized coherent states centered at (q, p) as follows:

$$c_{(q,p),k}(s) = \sum_{m\in\mathbf{Z}} \exp[i\,k\,p\,(s-q+m\,L)] \times \exp\left[-\frac{k}{2}(s-q+m\,L)^2\right]. \tag{5}$$

The Poincaré-Husimi function is then defined as the absolute square of the projection of the boundary function $u_m(s)$ onto the coherent state, namely,

$$H_m(q,p) = \left|\oint c_{(q,p),k_m}(s)\,u_m(s)\,ds\right|^2, \tag{6}$$

where $u_m(s)$ is the boundary function, which is the normal derivative of the eigenfunction of the mth state $\psi_m(\mathbf{r})$ on the boundary at point s,

$$u_m(s) = \mathbf{n}\cdot\nabla_{\mathbf{r}}\psi_m[\mathbf{r}(s)]. \tag{7}$$

Here, $\mathbf{n}$ is a unit outward normal vector to the boundary at point $\mathbf{r}(s)$. The boundary function satisfies an integral equation and also uniquely determines the value of the wave function $\psi_m(\mathbf{r})$ at any interior point $\mathbf{r}$ inside the billiard $\mathcal{B}$.

According to the principle of uniform semiclassical condensation (PUSC) of the Wigner functions and Husimi functions (see [5,22] and the references therein), the PH functions are expected to condense (collapse) in the semiclassical limit either on an invariant torus or on the chaotic component in the classical phase space. This is exactly what we observe—the higher the energies, the sharper the condensation or collapse of the PH functions. At not sufficiently high energies, *mixed-type eigenstates (PH functions)* may exist due to the tunneling between regular and chaotic domains (see [18,53] and references therein), but their number is expected to decrease monotonically with increasing e.

IV. SEPARATING REGULAR AND CHAOTIC EIGENSTATES

We use the PH functions to identify regular and chaotic eigenstates, simply by the criterion of overlap with the classical invariant tori or the chaotic region, respectively. This has been introduced and implemented in our previous papers [47,54]; see, also, Refs. [21,22]. There we have defined an overlap index M, which in the ideal case is $+1$ for chaotic states and -1 for regular states. Namely, we discretize the classical phase space (q, p) and the quantum phase space defined by the PH functions $H(q, p)$ into a rectangular grid of points indexed by (i, j) centered in cells of equal area, and normalize the PH functions in such a way that $\sum_{i,j} H_{i,j} = 1$. At each grid point, we define a discrete quantity $C_{i,j}$ such that it is $+1$ if the grid point (i, j) belongs to the chaotic region, and -1 otherwise. The chaotic region is constructed and generated by a single sufficiently long and dense chaotic orbit. This implies that the complement contains all the regular regions and possibly the other smaller chaotic regions. Typically, these smaller chaotic regions are so small that they can be neglected and treated as if they belonged to the regular part.

We calculate the overlap index M as follows:

$$M = \sum_{i,j} H_{i,j}\,C_{i,j}. \tag{8}$$

Ideally, in the sufficiently deep semiclassical limit, M should obtain either exact value $+1$ or -1, for the chaotic or regular type of the PH function, respectively. In practice, since the semiclassical limit is not yet achieved, M also assumes values between $+1$ and -1. The question arises as to what value $M = M_s$ should be taken as the criterion to separate the regular and chaotic eigenstates. In the past [47,54], we have used two possible physical criteria: (i) the classical one and (ii) the quantum one. In the former case, we choose M_s such that the fractions of regular and chaotic states are the classical values ρ_r and $\rho_c = 1 - \rho_r$, respectively. The quantum criterion for M_s is such that the fit of the chaotic level spacing distribution best agrees with the Brody distribution. This method is applicable in a general case. In Sec. VI, we will analyze the distributions of the overlap index in relation to the localization measures and show that the number of mixed-type eigenstates (their PH functions), with intermediate values of M, monotonically decreases with increasing energy as expected in the Berry-Robnik picture.

V. LOCALIZATION MEASURES

Following our previous papers, e.g., [54] (see, also, [33]), we will now introduce the localization measures for PH functions. They are special cases of the more general localization measures based on Wehrl entropy [55], also recently studied in Refs. [56–58]. We define the *entropy localization measure of a single eigenstate—of its PH function—$H_m(q, p)$* as

$$A_m = \frac{\exp I_m}{N_c}, \tag{9}$$

where

$$I_m = -\int dq\,dp\,H_m(q,p)\ln[(2\pi\hbar)^f H_m(q,p)] \tag{10}$$

is the information entropy of the eigenstate m. Here, f is the number of degrees of freedom [for two-dimensional (2D) billiards $f = 2$, and for surface of section it is $f = 1$] and N_c is a number of Planck's cells on the classical domain, $N_c = \Omega/(2\pi\hbar)^f$, where Ω is the classical phase space volume. In the case of the uniform distribution (extended eigenstates), $H = 1/\Omega = \text{const}$, the localization measure is $A = 1$, while in the case of the strongest localization, $I = 0$ and

$A = 1/N_C \approx 0$. The Poincaré-Husimi function $H(q, p)$ (6) (normalized as mentioned before) was calculated on the grid points (i, j) in the phase space (q, p), and we express the localization measure in terms of the discretized function $H_{i,j}$ as follows:

$$A_m = \frac{1}{N} \exp\left(-\sum_{i,j} H_{i,j} \ln H_{i,j}\right), \tag{11}$$

where N is the number of grid points of the rectangular mesh with cells of equal area. We have $H_{i,j} = 1/N$ in the case of complete (constant) extendedness, and $A = 1$. In the case of maximal localization, we have $H_{i,j} = 1$ at just one point, and zero elsewhere, yielding $A = 1/N \approx 0$ for large N. In all calculations, we have used the grid of 1000×750 points, and thus $N = 750\,000$.

According to this definition, regular eigenstates that condense on invariant tori are localized. The distribution of the localization measures $P(A)$ for these regular states is close to linear, starting from small $A \approx 0$ and increasing up to a maximal cutoff value $A = A_c$, corresponding to the outermost torus (last torus) of the regular island as explained in [33]. This applies to each possible chain of regular islands.

The chaotic PH functions can be either strongly localized or extended, but never entirely uniformly extended (i.e., not uniformly constant), as they experience oscillations and display a characteristic pattern of their nodal (zero level) points [37,59]. Therefore, the maximal value of A, denoted by A_0, is approximately $A_0 \approx 0.7$ according to empirical studies with real energy spectra [33]. The random wave-function model yields numerically $A_0 \approx 0.694$ [45], while a theoretical estimate of the random wave-function model in the *ultimate semiclassical limit* yields (see Refs. [58,60–63]) $A_0 = e^{(\gamma-1)} \approx 0.65\,522$, where $\gamma = 2.71\,828$ is the Euler constant. In mixed-type systems, the upper bound of the measure will be further reduced compared to fully chaotic ergodic systems since not all of the phase space is accessible. One must renormalize and divide the measured A by the relative area χ_c of the chaotic component in the phase space to make a quantitative comparison for the upper bound in the two different settings, as was done in our previous work. In this work, we examine regular, chaotic, and mixed states and will not rescale the measures of the chaotic states and keep the definition given by Eq. (9) for all types of states.

Of course, one may define many localization measures that are more sensitive to different features of the underlying PH functions. In the literature, many possibilities are presented, and the most general definition is based on the Renyi entropy (see Refs. [56,58]) of class α. $\alpha = 1$ corresponds to the information (Shannon) entropy on which the localization measure A in Eq. (9) is based. Another localization measure is the normalized inverse participation ratio R corresponding to $\alpha = 2$. Here we define it as follows in terms of the discretized and normalized Poincaré-Husimi function:

$$R = \frac{1}{N \sum_{i,j} H_{i,j}^2}. \tag{12}$$

$R = 1/N$, where N—the number of grid points—is very large, corresponds to the maximal localization $R \approx 0$, while $R = 1$ corresponds to the full extendedness [delocalization, where $H_{i,j} = 1/N$ for all (i, j)]. At this point, it is useful to discuss the differences between the measures A and R and develop some intuitive understanding. As already discussed, both measures are sensitive to the overall "size" or "extendedness" of the PH function in the phase space. However, taking a logarithm of the PH function as in A will suppress the differences in the magnitudes between the high-intensity and low-intensity areas, whereas taking a square of the PH function further enhances the peaks where $H_{i,j} > 1$ and suppresses the low-intensity background where $H_{i,j} < 1$. The measures will thus produce the most distinct results for PH functions that are strongly peaked in just a small area, but have a much larger support. This makes the measure especially suitable for finding states scarred by periodic orbits, as demonstrated for the Dicke model by Pilatowsky-Cameo *et al.* in Ref. [63] and in triangular billiards [64]. In previous works [49,50], we have shown that after a local averaging in energy, the relationship between A and R for chaotic states is linear. Here we explore the relationship further by examining the joint probability distribution density $P(A, R)$, which is the probability of finding an eigenstate within an infinitesimal box $[A, A + dA] \times [R, R + dR]$. We normalize the distributions on the rectangle $(A, R) \in [0, 0.4] \times [0, 0.3]$.

Let us first consider the $B = 0.1953$ lemon billiard, with the comparatively simpler phase space featuring three stable island chains. In Fig. 6, we show the joint probability distribution density $P(A, R)$ as a color plot, together with some representative PH functions from different regions of the parameter space. The PH functions are selected as the highest-energy eigenstate found in a local area of the plot. Let us first focus only on the distribution presented in the central figure. The white areas are regions where no eigenstates are found. We immediately notice that the distribution is supported only on a small area near the diagonal of the rectangle. This corroborates the previously known result that the localization measures A and R are, on average, linearly related. We also observe two main clusters of eigenstates (note that the color scale is logarithmic): a very sharp peak supported on a nearly one-dimensional line segment and a wider peak in the more delocalized regime. The first cluster is formed by the regular states localized on the invariant tori of the islands of stability, as can clearly be seen by examining some representative PH functions presented in Figs. 6(a) and 6(b). The second cluster is formed by the chaotic eigenstates, with representative examples given in Figs. 6(g), 6(h), 6(i), and 6(l) on the periphery. We will refer to the two clusters as the regular and chaotic cluster, respectively. They are visibly connected by additional structures. Outside the main clusters, many interesting mixed states may be found. Figures 6(c) and 6(d) show tunneling states between two of the outer tori of different island chains. These states are interesting because they can support chaos-assisted tunneling [19]. The states shown in Figs. 6(e), 6(f) 6(j), and 6(k) represent chaotic states with a significant overlap with boundary tori, signifying tunneling between the chaotic and regular component. Although one would need to classify each state individually for a full description, the distribution together with the representative PH functions provide a good overview of the phenomenology of the eigenstates. One may also notice that some mixed states, e.g., Figs. 6(c) and 6(d), belong to much lower wave

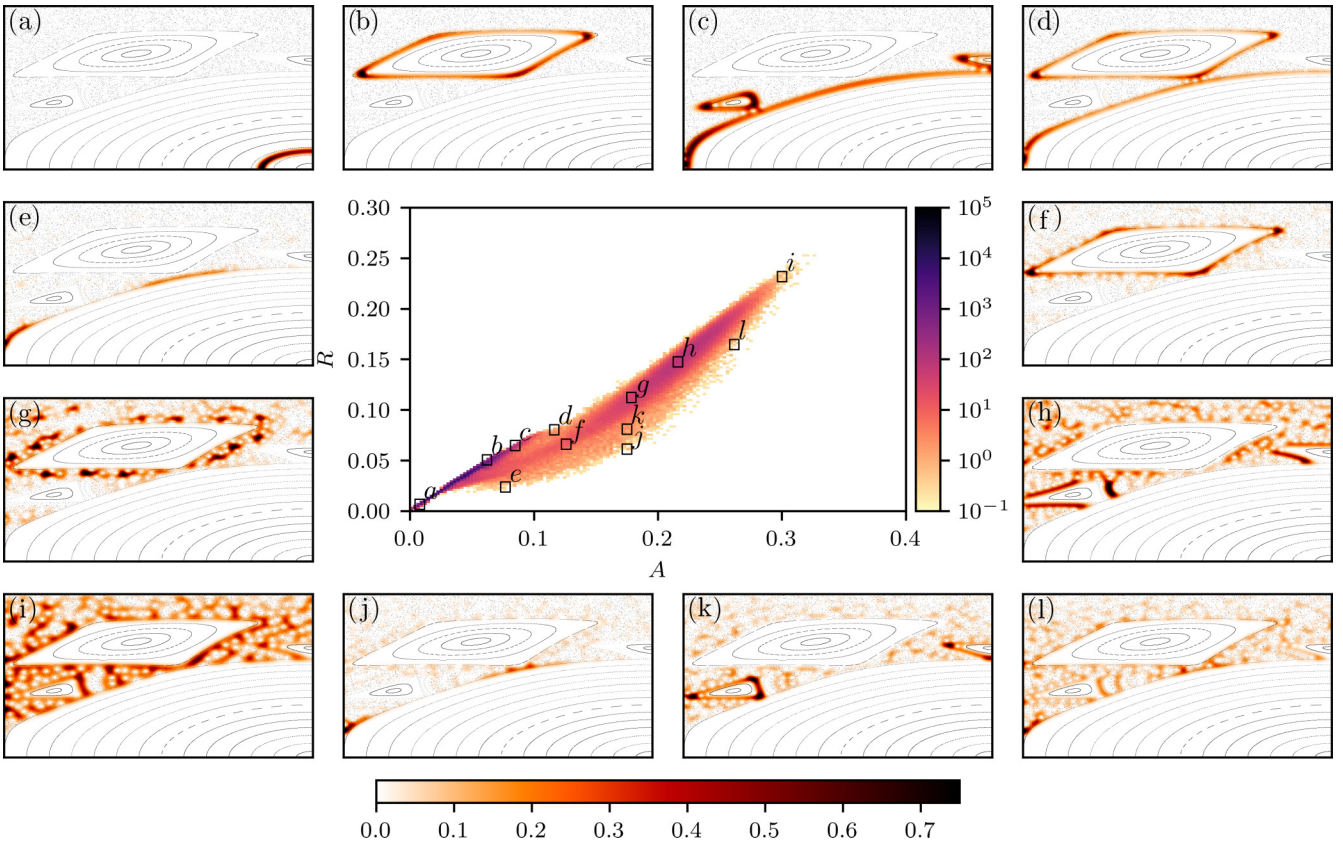

FIG. 6. Center: Color plot of the histogram of the joint probability density $P(A, R)$ for approximately 10^6 eigenstates with unfolded energy $e \in [10^4, 10^6]$ of the $B = 0.1953$ lemon billiard. The color scale of the main figure is logarithmic. PH functions of the highest-energy eigenstates within small boxes at various positions are shown on the margin. Their corresponding wave numbers are (a) $k = 4638.3906$, (b) $k = 4131.8411$, (c) $k = 2839.9081$, (d) $k = 3889.6615$, (e) $k = 4609.8260$, (f) $k = 4637.4242$, (g) $k = 4636.6707$, (h) $k = 4638.1850$, (i) $k = 2813.2003$, (j) $k = 4471.7931$, (k) $k = 4629.2434$, and (l) $k = 4501.5252$. A classical phase portrait is plotted in the background of each state for comparison. The color scale at the bottom encodes the relative amplitude of the PH function.

numbers since states in this area cease to exist after a certain energy is reached. We will more thoroughly present the energy dependencies in Sec. VII.

We now compare the results from the $B = 0.083$ lemon billiard, with the much more elaborate island structure, presented in the same manner in Fig. 7. The same basic close to diagonal structure, with two main clusters, may be seen. However, the exact positions of the structures are different. This is not unexpected since the localization measures are sensitive to the geometry of the phase space and sizes of the tori, islands, and chaotic component. The chaotic cluster is moved towards lower values of the localization measures since the relative size of the chaotic component is smaller, but also because of dynamical localization effects that may be seen in the PH functions portrayed in Figs. 7(d)–7(f). The state shown in Fig. 7(f) is also highly peaked near the boundary of the largest island of stability and might be interpreted as a mixed state describing tunneling between the three nearby island chains. The state shown in Fig. 7(g) has strong peaks in the same areas, but extends weakly across the whole of the chaotic component. The states shown in Figs. 7(h)–7(l) are extended chaotic states of various uniformity. However, some flooding into islands of stability is clearly visible. In particular, the states shown in Figs. 7(j) and 7(k) flood the topmost islands of stability completely and partially overlap other islands. Complete flooding of the topmost islands is also observed in the localized state shown in Fig. 7(e). The states shown in Figs. 7(a)–7(c) are regular eigenstates and are typical examples of states from the regular cluster.

To summarize, the joint probability distributions $P(A, R)$ are structurally similar in both example billiards. They feature two main clusters of states: the regular cluster supported on a very narrow strip (practically a line segment) and a wider chaotic cluster. The wide majority of states is found in these two clusters. The mixed states are found on the margins of the clusters and on an additional system-specific structure connecting the two main clusters that are related to the various tunneling processes between different island chains and the chaotic component. It is perhaps surprising that this much insight into the structure of the phase space may be gained by studying the relation between two simple localization measures of the same object, the PH function. The major advantage of this approach is that no prior information of the classical phase space is necessary. This may be of vital importance when studying higher-dimensional systems, where the classical computations and production of detailed phase space portraits become increasingly difficult. In particular, the regular states are very easily identifiable since they cluster on such a narrow part of the parameter space.

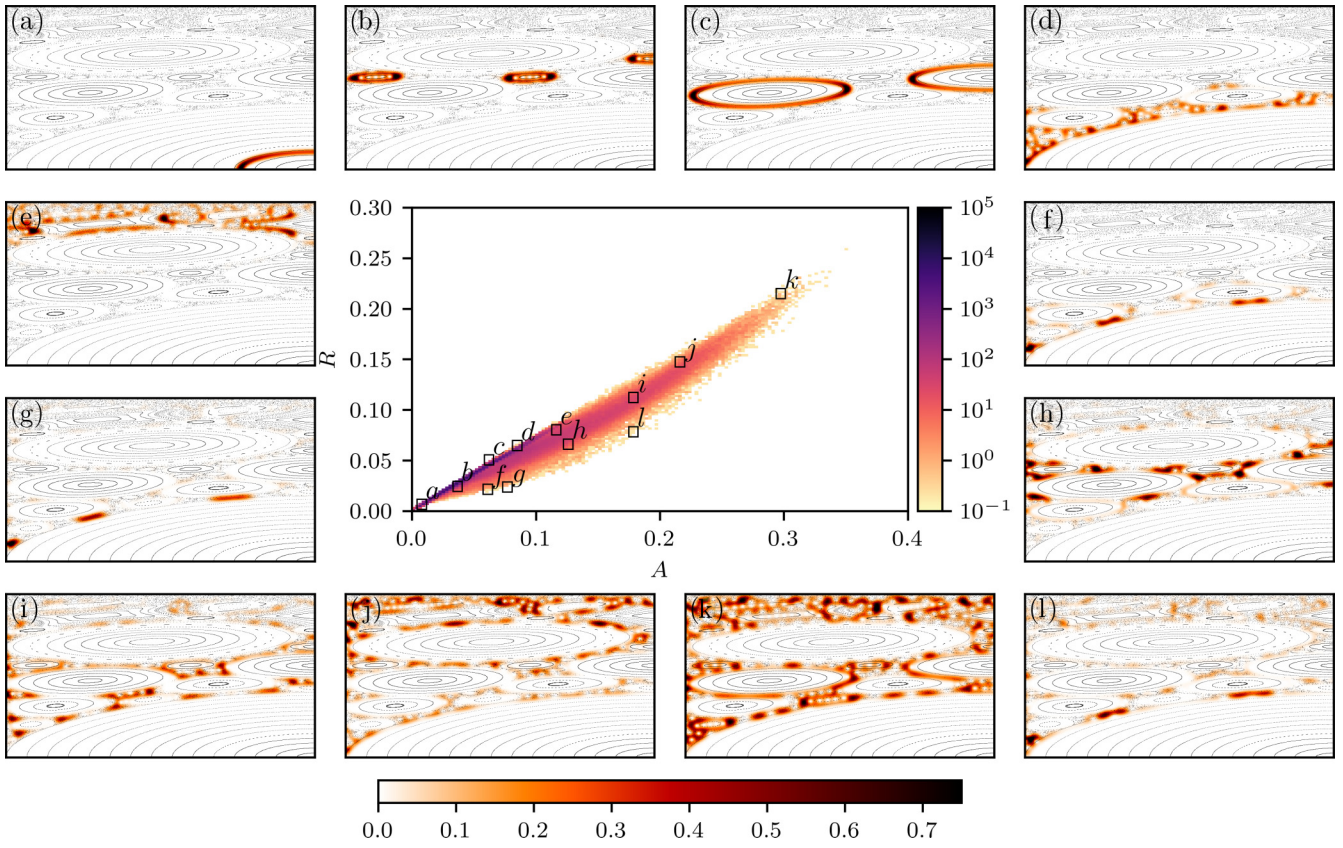

FIG. 7. Center: Color plot of the histogram of the joint probability density $P(A, R)$ for approximately 10^6 eigenstates with unfolded energy $e \in [10^4, 10^6]$ of the $B = 0.083$ lemon billiard. The color scale of the main figure is logarithmic. PH functions of the highest-energy eigenstates within small boxes at various positions are shown on the margin. Their corresponding wave numbers are (a) $k = 4255.7099$, (b) $k = 4255.6717$, (c) $k = 4255.6550$, (d) $k = 4253.5121$, (e) $k = 4255.5289$, (f) $k = 4251.1624$, (g) $k = 4253.4432$, (h) $k = 4255.0162$, (i) $k = 4255.6096$, (j) $k = 4254.0484$, (k) $k = 3318.7134$, and (l) $k = 3927.8888$. A classical phase portrait is plotted in the background of each state for comparison. The color scale at the bottom encodes the relative amplitude of the PH function.

VI. OVERLAP INDEX AND LOCALIZATION MEASURES

The classical computations presented is Sec. II enable us to easily compute the overlap index of the classical chaotic and regular components and the PH functions, given by Eq. (8). This is information about the relative overlap with the classical structures, but this alone is not sufficient to identify the processes leading to only partial overlap. We therefore compare the overlap index of each individual state and its localization measures and study the joint probability distributions $P(A, M)$ and $P(A, R)$. We will focus on the distributions $P(A, M)$, that is, the probability of finding a state within an infinitesimal box $[A, A + dA] \times [M, M + dM]$. We normalize the distributions on the rectangle $(A, M) \in [0, 0.4] \times [-1, 1]$.

In Fig. 8, we show the joint probability distribution density $P(A, M)$ in the $B = 0.1953$ as a color plot, together with some representative PH functions from different regions of the parameter space. The PH functions are selected as the highest-energy eigenstate found in a local area of the plot, and the color scale is logarithmic. The regular states belonging to the inner invariant tori form a sharp cluster at $M = -1$, extending to $A \approx 0.075$. An example is shown in Fig. 8(k), as well as an extreme example with tunneling between two invariant tori in Fig. 8(l). The chaotic states form a larger cluster with $M \gtrsim 0.8$. Clearly, quite many chaotic states still have a small overlap with the outer tori of the regular islands, but can nevertheless be interpreted as purely chaotic states. On the A axis, the chaotic cluster extends over a relatively large range from $A \approx 0.1$ to $A \approx 0.3$. The states shown in Figs. 8(a)–8(c) show the transition from localized to increasingly uniform chaotic states. The regular and chaotic clusters are connected continuously by the mixed states. Going from the chaotic towards the regular cluster, we see various tunneling processes such as between the outer tori and the chaotic component shown in Figs. 8(d)–8(f), and also including outer tori of different island chains, shown in Fig. 8(g). In the lower part of the diagram $M < -0.5$, we see three structures of greater density. They correspond to states condensed on the boundary tori of the three island chains $\mathcal{L}$, $\mathcal{S}$, and $\mathcal{M}$, as is evident from the PH functions shown in Figs. 8(h)–8(j), correspondingly. These states should be classified as regular. We have thus shown that the joint probability distribution $P(A, M)$ gives an excellent phenomenological overview of this mixed-type system.

Figure 9 shows the distribution $P(A, M)$ in the other lemon billiard $B = 0.083$. It is evident that the separation based on the values of M is not so simple. The billiard $B = 0.083$ has a much more complex classical phase portrait (see Figs. 4 and 5). While the purely regular states on the inner invariant tori again form a sharp cluster at $M = -1$, the chaotic states are

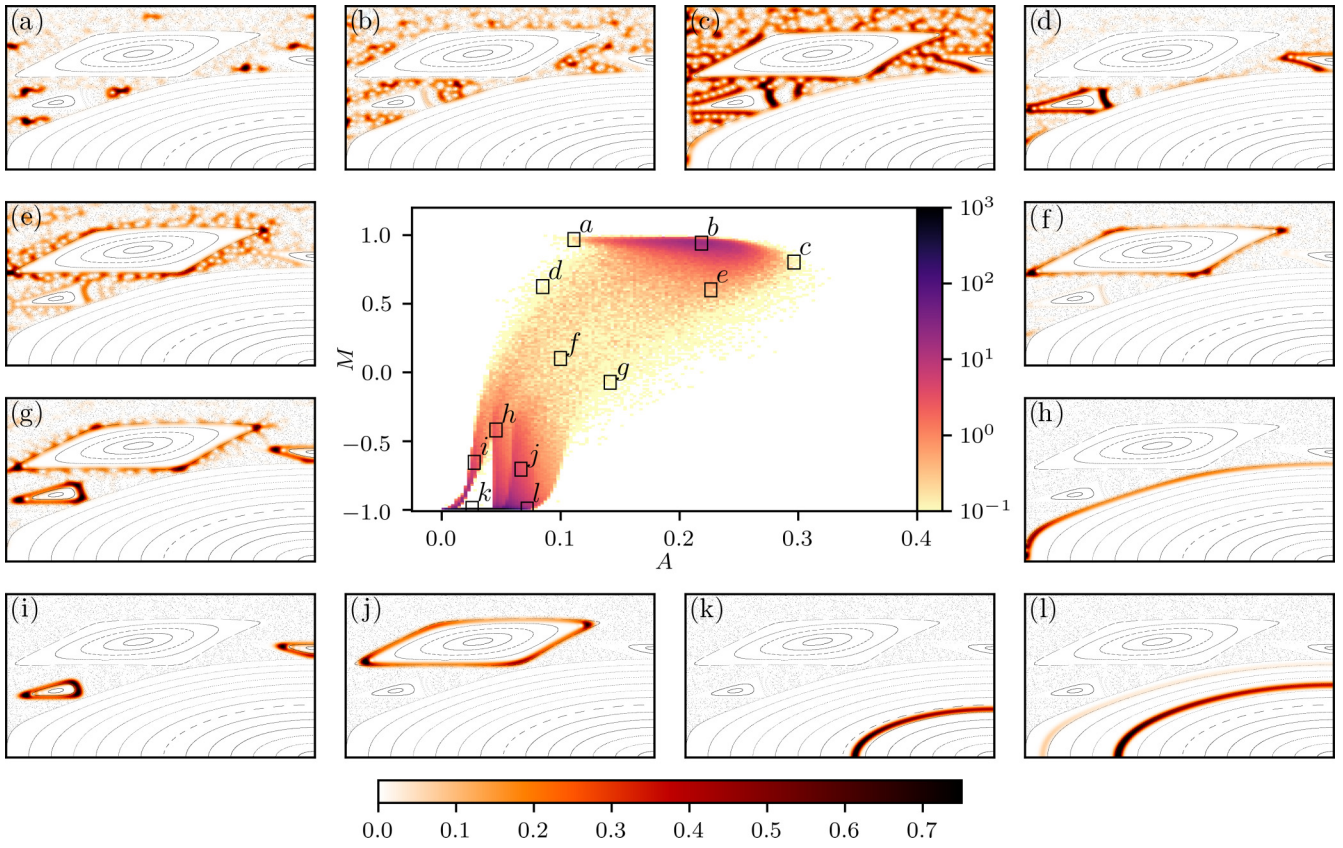

FIG. 8. Center: Color plot of the histogram of the joint probability density $P(A, M)$ for approximately 10^6 eigenstates with unfolded energy $e \in [10^4, 10^6]$ of the $B = 0.1953$ lemon billiard. The color scale of the main figure is logarithmic. PH functions of the highest-energy eigenstates within small boxes at various positions are shown on the margin. Their corresponding wave numbers are (a) $k = 4598.5120$, (b) $k = 4638.3417$, (c) $k = 3486.3962$, (d) $k = 4637.4426$, (e) $k = 4610.3436$, (f) $k = 4603.9386$, (g) $k = 4050.5505$, (h) $k = 4636.9990$, (i) $k = 4637.1017$, (j) $k = 4236.8109$, (k) $k = 4638.4472$, and (l) $k = 3776.8166$. A classical phase portrait is plotted in the background of each state for comparison. The color scale at the bottom encodes the relative amplitude of the PH function.

quite uniformly distributed over a wider range of M values. Similarly to the previous example, the regular states of the outer tori of the different island chains form higher-density "ridges" in the distribution. Because of the complexity of the phase space, there are now many of them, each corresponding to a chain of islands. Some of these outer tori states may be seen in the examples of Figs. 9(j) and 9(k), as well as Fig. 9(l), where we see tunneling between two nearby island chains. Progressing upwards towards the chaotic regime, the states shown in Figs. 9(h) and 9(i) exhibit tunneling between the outer tori and the chaotic sea. Crossing over into the predominantly chaotic regime $M > 0$, we find some very localized states shown in Figs. 9(a) and 9(e)–9(g), and some increasingly extended states shown in Figs. 9(b)–9(d). The relatively small values of the overlap index are caused mainly by the flooding into the islands of stability, seen already in the joint localization measure distributions for this billiard ($B = 0.083$). The mixed-type states are still strongly represented, their number decreases with increasing energy e, but they would disappear only at much higher energies. Purely chaotic states are practically nonexistent in this energy range, although their expected relative fraction is classically $\rho_2 = 0.1617$.

Although there are subtle differences between the localization measures A and R (analyzed in the previous section), the general behavior of both is the same. For comparison, we show the distributions $P(R, M)$ in Fig. 10.

VII. ENERGY DEPENDENCE AND THE SEMICLASSICAL CONDENSATION

In the semiclassical limit, we expect that the mixed chaotic regular states will gradually disappear in keeping with Berry-Robnik picture and PUSC. To study this, we consider the localization measures and overlap indices of eigenstates in narrower energy intervals, starting at progressively higher energies. Let us first inspect how the joint localization measure distributions $P(A, R)$ change with increasing the energy and progressing deeper into the semiclassical limit. This is shown in Fig. 11 for both billiards. The invariant tori are one-dimensional objects in the phase space. When the energy is increased, the PH functions of the regular states condense on the invariant tori and become ever thinner and the localization measures of the regular states are decreased. The chaotic sea, on the other hand, is a positive measure set. In the final semiclassical regime, we would expect to see a δ-distribution-like peak at $(A, R) = (0, 0)$ containing ρ_1 (the relative classical Liouville measure of the regular components) and another peak containing the $\rho_2 = 1 - \rho_1$ chaotic states at $A = A_0$ and $R = R_0$. The exact position of the chaotic peak at (A_0, R_0)

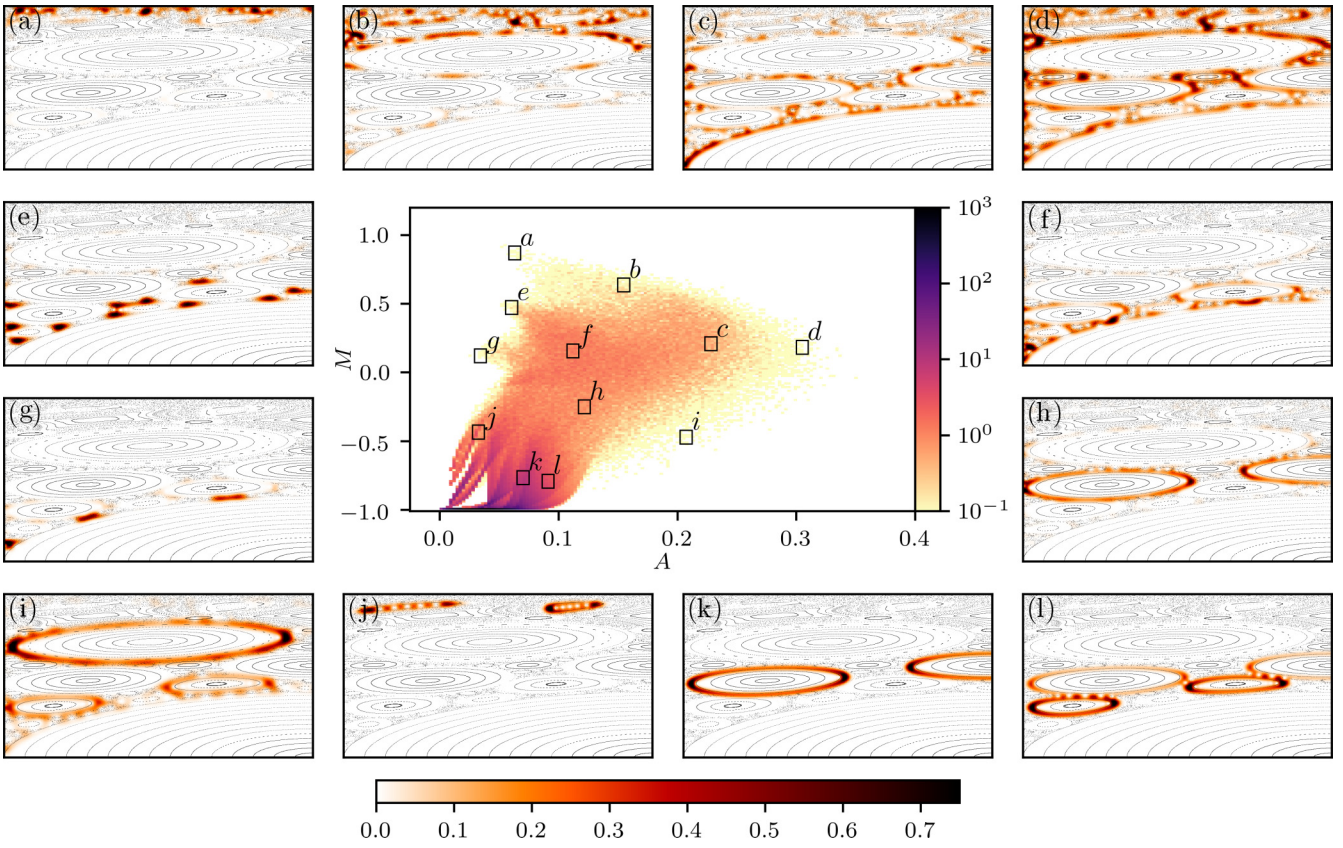

FIG. 9. Center: Color plot of the histogram of the joint probability density $P(A, M)$ for approximately 10^6 eigenstates with unfolded energy $e \in [10^4, 10^6]$ of the $B = 0.083$ lemon billiard. The color scale of the main figure is logarithmic. PH functions of the highest-energy eigenstates within small boxes at various positions are shown on the margin. Their corresponding wave numbers are (a) $k = 4221.4610$, (b) $k = 4253.9880$, (c) $k = 4227.7699$, (d) $k = 2649.8961$, (e) $k = 4250.2980$, (f) $k = 4254.5877$, (g) $k = 4113.9895$, (h) $k = 4254.0666$, (i) $k = 2126.9352$, (j) $k = 4255.2063$, (k) $k = 4255.6550$, and (l) $k = 4181.7921$. A classical phase portrait is plotted in the background of each state for comparison. The color scale at the bottom encodes the relative amplitude of the PH function.

will depend on the measure of the chaotic component and the geometry of the phase space. In the $B = 0.1953$ billiard (top row of Fig. 11), the chaotic and regular clusters are already distinguishable in the lowest-energy interval, starting with $e = 10^4$, although there are still many intermediate mixed states forming a smooth transition between them (we must keep in mind that the color scales are logarithmic and as such reduce the contrast between the different orders of magnitude). As we increase the starting energy, the mixed states gradually disappear, the features of the distribution $P(A, R)$ become sharper, and a gap between the regular and chaotic states starts to open. The localization measures of the chaotic states (the center of the chaotic cluster) remain roughly the same with increased energy. Even though the semiclassical limit, with no mixed regular-chaotic states, is not yet achieved, the trend towards this regime is evident. The joint distributions for the $B = 0.083$ billiard are still further away from the semiclassical regime, owing to the greater complexity of the phase space. The center of the chaotic cluster is located at lower values of the localization measure since the chaotic sea of this system is very thin. Flooding effects and dynamical localization are also present, as we observed in the representative PH functions in Secs. V and VI. All this contributes to the fact that only a slight indication of a gap opening between the chaotic and regular states is visible in the color plots.

The semiclassical condensation is even more evident when observing the energy dependence of the joint probability distributions $P(A, M)$. The distributions for different energy intervals are presented in Fig. 12. In the $B = 0.1953$ billiard, separation of the chaotic and regular eigenstates is very clear, and the mixed states become ever scarcer as we increase the energy. The three structures containing the outer tori of the three island chains also become very sharply defined. In accordance with our previous findings, the separation of the chaotic and regular states in the $B = 0.083$ billiard is more ambiguous. However, we can still very clearly see the condensation of the states on the outer invariant tori of the many island chains and that mixed states, especially at $M < 0$, appear less abundant. To quantify the decay of mixed states, we consider the following quantity. We define some interval in M that we believe corresponds to the mixed states. Although this interval is somewhat arbitrary, the qualitative analysis of the PH functions may give an informed opinion on what values to take in each case. We then take an energy interval of width w starting at e and count the number of mixed states and divide by the number of all states in the interval. We observe the decay of this relative proportion of mixed states labeled $\chi_M(e)$ as a function of energy and also the interval taken in M. We find that for mixed states, this quantity decays asymptotically as a power law $\chi_M(e) \propto e^{\gamma}$, where the

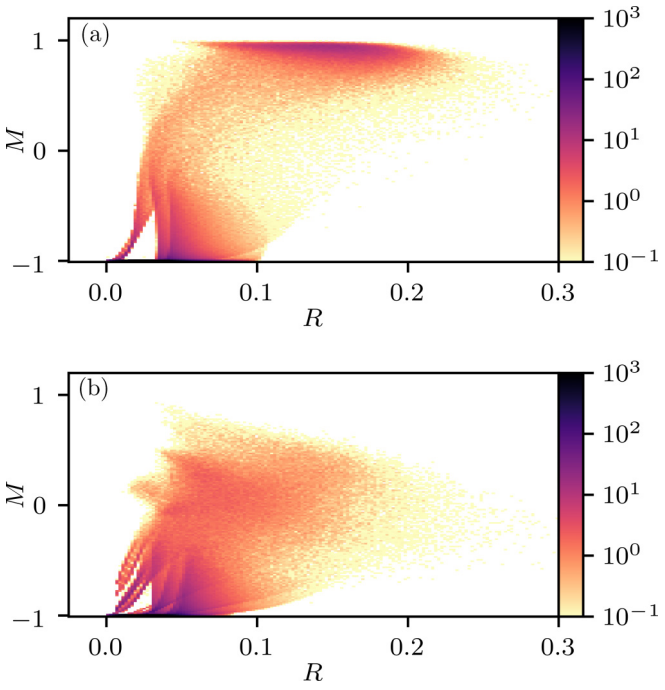

FIG. 10. Center: Color plot of the histogram of the joint probability density $P(R, M)$ for approximately 10^6 eigenstates with unfolded energy $e \in [10^4, 10^6]$ of the (a) $B = 0.1953$ and (b) $B = 0.083$ lemon billiard. The color scale is logarithmic.

exponent $\gamma < 0$ depends on the interval we take in M. From the visual inspection of the PH functions (see Figs. 8 and 9), we determined that the mixed states are contained in the interval $M \in [-0.8, 0.8]$ for the $B = 0.1953$ and $M \in [-0.8, 0.1]$ for the $B = 0.083$ billiard. We found that taking $w = 10^4$ gives us a good compromise between the energy resolution and statistical significance for the relative number of states contained in the interval. In Fig. 13(a), we show the decay of the relative number of mixed states when taking the maximum interval in M for each billiard. The decay rate is similar for both billiards, $\gamma = -0.29$. Similar power-law decays may also be seen when considering smaller intervals in M. In Fig. 13(b), we show the change of the decay exponent when taking relatively small intervals $[M, M + \delta M]$ with $\delta M = 0.1$. The decay exponents show a transition from $\gamma \approx -0.15$ to $\gamma \approx -0.5$ with increasing M. This indicates that the number of states related to the flooding processes decays faster than that of the states related to the tunneling from regular islands. The transition is similar in both billiards, but is slightly displaced in the $B = 0.083$ case.

VIII. SUMMARY, DISCUSSION, AND CONCLUSION

In the present paper, we have investigated two lemon billiards with complex classical phase portraits of the mixed type, exhibiting a dominant uniform classical chaotic component and several chains of regular islands. The choice $B = 0.1953$ and $B = 0.083$ is based on the systematic survey of the large family of lemon billiards in Ref. [30]. The two billiards were singled out due to the complexity of the phase space and the absence of any apparent domains of stickiness, as shown by the classical computations of recurrence time statistics. Our study is focused on the quantum mechanics of these billiards. In the present paper, we have presented a detailed analysis of the eigenstates in the Poincaré-Husimi representation and a phenomenological study, which gives a very good overview of all types of eigenstates, from regular to chaotic and mixed.

To summarize our main results: (i) We analyze the joint probability distributions of Reny-Wehrl localization measures of different orders of the eigenstates, revealing characteristic structures related to the regular chaotic and mixed eigenstates and quantifying their prevalence. (ii) We analyze the joint probability distributions of Reny-Wehrl localization measures in relation to a simple overlap measure with the classical phase space. The structure of the joint probability distribution allows for an even easier interpretation of chaotic, mixed, and regular states. Different tunneling processes may be identified, for instance, states on the boundary of the islands of stability (last invariant tori), states that support chaos-assisted tunneling between islands, chaotic states that flood into islands of stability, etc. (iii) We analyze the transition into the Berry-Robnik regime as a function of energy and show that the fraction of mixed eigenstates decreases as a power law. The exponent depends on the type of tunneling process and ranges from -0.2 to -0.5.

A preliminary survey of the spectra of the two lemon billiards was published in Ref. [34], where the fluctuation of the number of the energy levels (mode fluctuation) was shown to obey the Gaussian distribution quite well. The level spacing distribution of the entire spectrum was shown to follow the Berry-Robnik-Brody (BRB) distribution. In the billiard $B = 0.1953$, the value of the level repulsion exponent β (Brody parameter) is close to 1, reflecting the absence of dynamical localization of the chaotic eigenstates, and the Berry-Robnik parameter ρ_r is close to its classical value. This is in line with the results of the current paper, where we see a very clear separation of the eigenstates at high energies in the same billiard. On the other hand, in the billiard $B = 0.083$, which has a much more complex phase space structure, the results for β and ρ_r fluctuate significantly from case to case for the four parities. A decrease of the level repulsion exponent has been linked to the presence of dynamically localized chaotic states [48,49], which we clearly observe in this billiard. The fluctuations of the Berry-Robnik parameter can also be explained since the energy-dependent joint probability distributions of the localization and quantum-classical overlap measures show that the asymptotic regime is not yet reached.

In the present paper, we presented an approach to interpret the localization measures by studying the joint probability distributions. We introduced two localization measures of individual PH functions, i.e., the entropy localization measure A and the normalized inverse participation ratio R, and the overlap index M, which measures the degree of overlap of the PH function with the regular and chaotic regions in the classical phase space. Ideally, in the strict semiclassical limit, $M = -1$ in purely regular regions and $M = 1$ in pure chaotic regions. In practice, we also find various eigenstates (PH functions) with $-1 < M < 1$, which belong to mixed states. We studied the joint probability distributions of all combinations of the measures, namely, $P(A, R)$, $P(A, M)$, and $P(R, M)$. Our analysis confirms that A and R are, on average, linearly

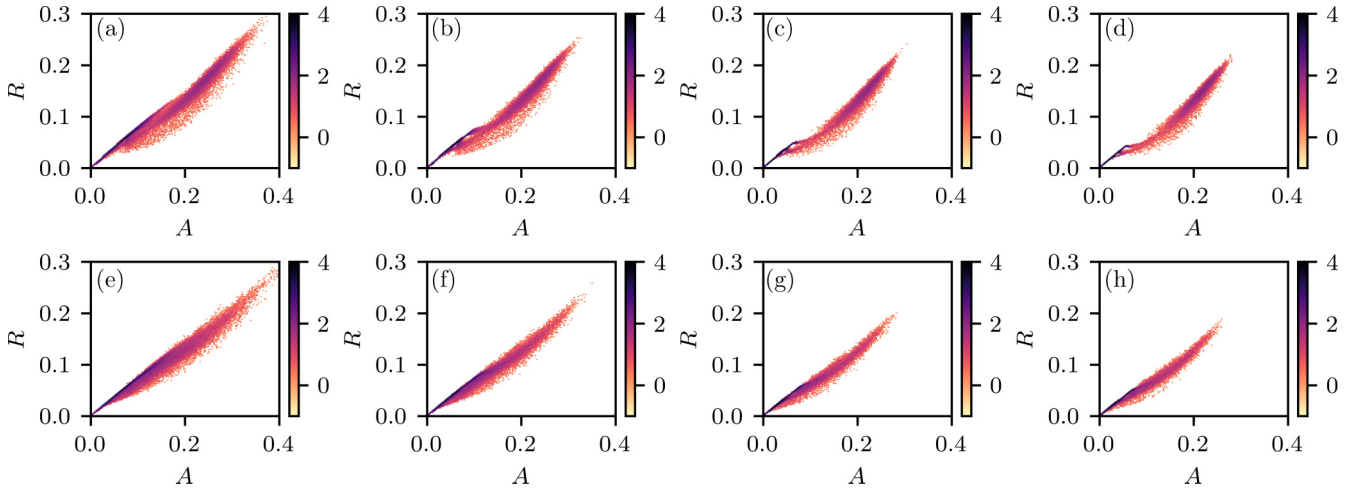

FIG. 11. Color plots of the histogram of the joint probability density $P(A, R)$ for approximately 10^5 eigenstates for progressively higher-energy intervals starting from (left to right) $e_0 = 10^4, 10^5, 5 \times 10^5, 9 \times 10^5$ for the $B = 0.1953$ (top row) and $B = 0.083$ (bottom row) lemon billiard. The color scale is logarithmic.

related. Therefore, the classification of states and the results on the statistical properties of the degree of localization for the chaotic states do not depend very much on the definition of the localization measure. However, subtle differences allow us to identify interesting mixed-type states and also distinguish between the regular and chaotic states based strictly on comparing the different localization measures, without considering the classical phase portraits. Indeed, measures based on higher-order Renyi entropy might also be considered to enhance the differences.

Very similar localization measures defined on different Hilbert space basis sets have been used to describe multifractality in random matrix models [65], many-body localized [66] and nonergodic extended states [67], the transition to chaos in interacting boson systems described by Bose-Hubbard Hamiltonians [68,69], and Anderson localization of Rydberg electrons interacting with ground-state atoms [70], to name some examples. Using the various definitions mentioned above, it would be possible to extend our approach and phenomenological descriptions to systems without a clearly defined classical limit. In particular, we propose to study the relations between the different orders of the localization measures in terms of joint probability distributions, as presented in this paper. The Berry-Robnik picture and the separation of eigenstates into regular and chaotic states is well established for noninteracting low-dimensional quantum systems with a well-defined semiclassical limit, and has been again demonstrated in the present paper. However, even classically, ergodicity and chaos is hard to prove when considering many-body interacting systems, as small, barely detectable islands of stability may persist. Naively, one expects that generic many-body interacting systems are ergodic and admit a statistical-mechanical description, yet these types of quantum systems may still display intermediate spectral statistics (between chaos and integrability). Weak ergodicity breaking has also been attributed to so-called many-body scarred states

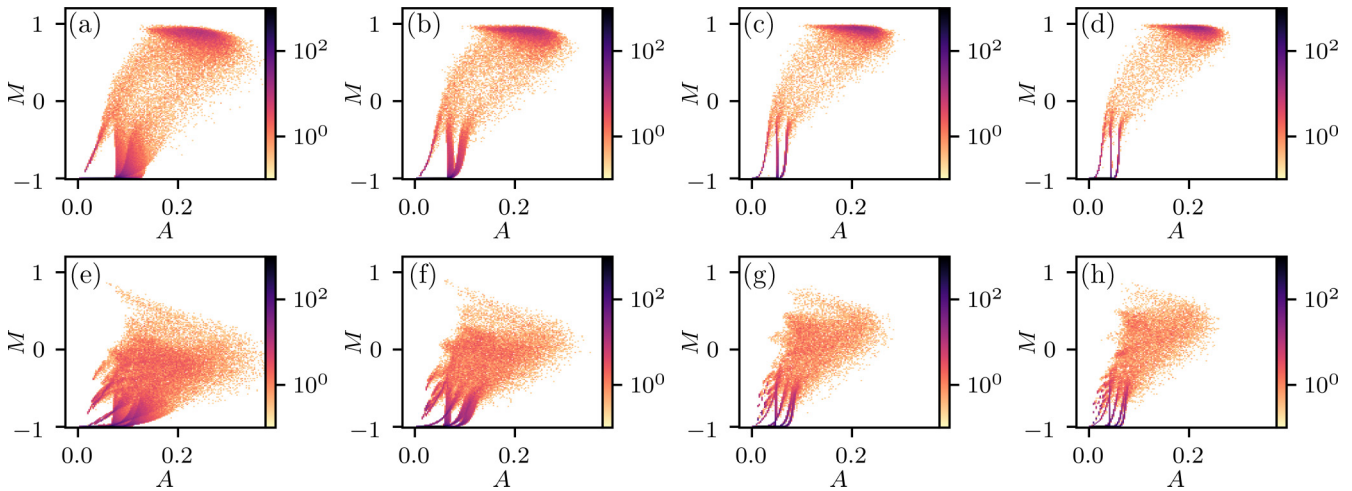

FIG. 12. Color plots of the histogram of the joint probability density $P(A, M)$ for approximately 10^5 eigenstates for progressively higher-energy intervals starting from (left to right) $e_0 = 10^4, 10^5, 5 \times 10^5, 9 \times 10^5$ for the $B = 0.1953$ (top row) and $B = 0.083$ (bottom row) lemon billiard. The color scale is logarithmic.

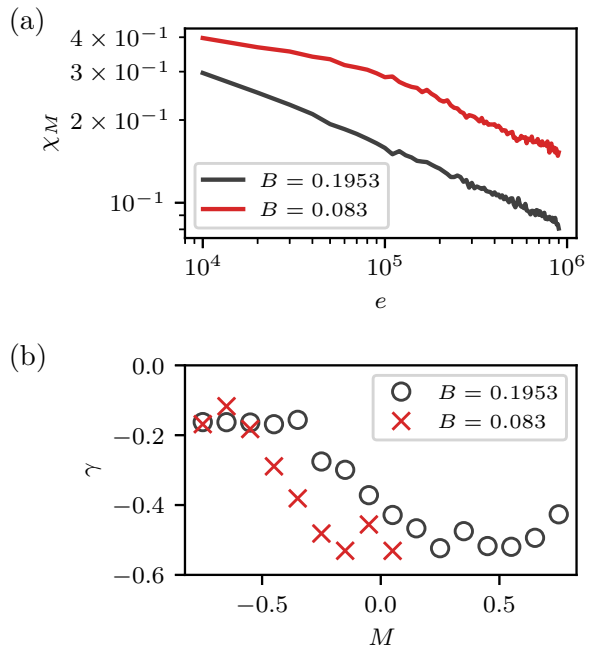

FIG. 13. Decay of the relative number of mixed states with energy. (a) The relative number of states in the interval as a function of unfolded energy. Both decay exponents are close to $\gamma = -0.29$. (b) Decay exponents for smaller intervals $[M, M + \delta M]$ with $\delta M = 0.1$.

[71]. It is not clear whether these states are associated with classical islands of stability, periodic orbit scarring, dynamical localization, or some other mechanism. Since clear structures associated with regular and chaotic states are visible in the joint probability distributions of the localization measures in our noninteracting example, it is feasible that some similar structures, if found in the many-body systems, would indicate the existence of states that are associated with islands of stability and would thus elucidate the many-body scarring mechanism. Further interesting research directions are possible in tight-binding billiard models [72], where it has been shown that the tight-binding billiard has similar ergodic properties to its continuous counterpart in the fully chaotic case.

To conclude, our study of the PH functions confirms that the Berry-Robnik picture of separation into regular and chaotic eigenstates is correct. The underlying mechanism is the principle of uniform semiclassical condensation of the Wigner functions (or PH functions) [5] that was developed from Percival's conjecture [2] and Berry's work [3,4]. The PH functions are asymptotically (in the ultimate semiclassical limit) either of the regular type or of the chaotic type. Mixed PH functions at lower energies exist and we have studied them in detail. We have shown that their number monotonically decreases with increasing energy in the semiclassical limit of high-lying eigenstates. Moreover, we have quantified this observation by showing that the relative fraction of mixed-type states decreases as a power law with increasing energy. This is the central result of our paper. Since billiards are a representative example of low-dimensional generic Hamiltonian systems, the approach is directly applicable to any quantum

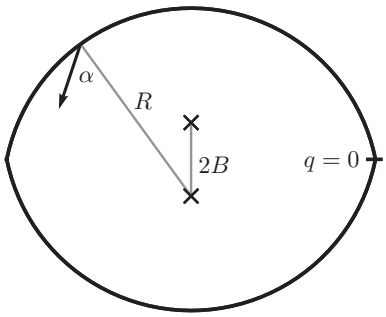

FIG. 14. Illustration of the lemon billiard geometry. Here, $B = 0.1953$

mixed-type Hamiltonian systems with a clear classical limit, such as the recently studied Dicke model [73], the kicked top model [74], or the three-site Bose-Hubbard model [75].

ACKNOWLEDGMENTS

We thank B. Georgeot, R. Ketzmerick, and L. Vidmar for elucidating discussions, T. Prosen for discussions and providing the extensive use of computational facilities, and M. T. Eiles for the careful reading of the manuscript. Č.L. thanks the MPG for its hospitality. This work was supported by the Slovenian Research Agency (ARRS) under Grant No. J1-9112.

APPENDIX A: LEMON BILLIARD GEOMETRY

The lemon billiards are defined by the intersection of two circles of equal unit radius with the distance $2B$ between their centers. The construction is illustrated in Fig. 14. In Cartesian coordinates, the boundary is given by the following implicit equations:

$$x^2 + (y + B)^2 = 1, \quad y > 0,$$
$$x^2 + (y - B)^2 = 1, \quad y < 0. \tag{A1}$$

To construct the canonical Poincaré-Birkhoff coordinates (q, p), we take the boundary as the surface of the section. The billiard dynamics (a series of line segments linking the collisions) is described by a series of points where the bounce position is given by the arclength q and the corresponding canonical momentum is $p = \sin(\alpha)$. We set the origin of the q coordinate into the right kink (corner) and integrate the length of the boundary counterclockwise up to the collision point. The period q is given by the circumference of the entire billiard boundary,

$$L = 4 \arctan \sqrt{B^{-2} - 1}. \tag{A2}$$

The area A of the billiard is equal to

$$A = 2 \arctan \sqrt{B^{-2} - 1} - 2B\sqrt{1 - B^2}$$
$$= \tfrac{1}{2}L - 2B\sqrt{1 - B^2}. \tag{A3}$$

To compute the fractional measure of the chaotic component, we will first compute the area χ_c, with one of the methods of Ref. [40], in the two-dimensional phase space (i.e., the surface of section in the Poincaré-Birkhoff coordi-

nates), and then calculate the Liouville measure in the full four-dimensional phase space. The relation between the two is given by the formula derived by Meyer [41],

$$\rho_c = \frac{\chi_c}{\chi_c + (1-\chi_c)\kappa}, \tag{A4}$$

where $\kappa = \frac{\langle t\rangle_r}{\langle t\rangle_c}$ is the ratio between the average return time to the surface of section (length of the trajectory between collisions divided by the speed of the particle) on the regular components $\langle t\rangle_r$ and the average of the same quantity on the chaotic component $\langle t\rangle_c$. For the equivalent formula pertaining to $\rho_r = 1 - \rho_c$, we only need to exchange the indices $r \leftrightarrow c$ and invert the ratio $\kappa \to 1/\kappa$ in Eq. (A4). In billiards, the surface of section is the billiard boundary and the ratio κ is independent of the speed of the particle. The surface of section return time is proportional to the length of a link of a trajectory between two consecutive collisions. The ratio κ is numerically computed by averaging the length of a link over a number of collisions and then computing the averages with regard to the initial conditions.

APPENDIX B: RECURRENCE TIMES AND STICKINESS

A generic mixed-type Hamiltonian commonly exhibits the phenomenon known as stickiness—chaotic orbits intermittently "stick" to islands of stability or other invariant structures for extended periods of time. This results in a slow (subexponential) decay of correlations and other observables such as recurrence times. Here, we will briefly outline the method for quantifying stickiness used to produce the S plots, based on the statistics of recurrence times. See [30,45] for a more in-depth explanation of the method and related results on stickiness. We consider the billiard system as a map, and thus the time is measured discreetly with the number of bounces (map iterations). Let $\mathcal{A}$ be an arbitrary subset of the phase space, for instance, a small cell $dq \times dp$. The first recurrence time to $\mathcal{A}$ for a point $a \in \mathcal{A}$ is defined as the number of iterations an orbit needs to return to the same cell for the first time,

$$\tau_{\mathcal{A}} = \min_{t>0}\{t : f^t(a) \in \mathcal{A}\}, \tag{B1}$$

where $f : (q, p) \to (q', p')$ is the bounce map. We are interested in the probability distributions of recurrence times. For chaotic systems, one expects the recurrences to be essentially uncorrelated, and thus the mean recurrence time is the inverse of the area of the test set (Kac's lemma) and the distribution is exponential. If we discretize the phase space into a grid of N_c cells,

$$P(\tau) = \frac{1}{N_c}\exp\left(-\frac{\tau}{N_c}\right). \tag{B2}$$

The assumption of completely uncorrelated cell recurrences is a strong one and, by definition, holds for so-called Bernoulli systems. Chaoticity in the sense of positive Lyapunov exponents is a weaker ergodic property. However, strong empirical evidence suggests that the recurrence times generically exhibit an exponential distribution in the bulk of the chaotic component, even in mixed-type systems, outside of the sticky areas. This is in agreement with the findings in the so-called random model [76]. Stickiness is a consequence of partial transport barriers such as cantori. The chaotic orbits become intermittently trapped, and thus short recurrences feature more prominently in the distribution. To quantify this effect, we exploit a special feature of the exponential distribution, namely, that its variance is equal to its mean, $\sigma = \mu$. The variable $S = \sigma/\mu$ (coefficient of variation) can thus distinguish between exponential and nonexponential distributions of recurrence times. When we consider small areas of the phase space (discretization cells), we may distinguish areas of uniform chaos $S = 1$ and sticky areas $S > 1$. The easiest way to generate the recurrence time statistics is to just run a sufficiently long chaotic orbit and track the S parameter locally in each cell.

[1] A. J. Lichtenberg and M. A. Lieberman, *Regular and Chaotic Dynamics* (Springer Verlag, New York, 1992).
[2] I. Percival, J. Phys. B: At. Mol. Phys. **6**, L229 (1973).
[3] M. V. Berry, J. Phys. A: Math. Gen. **10**, 2083 (1977).
[4] M. V. Berry, Philos. Trans. R. Soc. London, Ser. A, Math. Phys. Sci. **287**, 237 (1977).
[5] M. Robnik, Nonlin. Phenom. Complex Syst. (Minsk) **1**, 1 (1998).
[6] H.-J. Stöckmann, *Quantum Chaos—An Introduction* (Cambridge University Press, Cambridge, 1999).
[7] F. Haake, *Quantum Signatures of Chaos* (Springer, Berlin, 2001).
[8] M. V. Berry and M. Robnik, J. Phys. A: Math. Gen. **17**, 2413 (1984).
[9] T. Prosen and M. Robnik, J. Phys. A: Math. Gen. **26**, 5365 (1993).
[10] T. Prosen and M. Robnik, J. Phys. A: Math. Gen. **27**, L459 (1994).
[11] T. Prosen and M. Robnik, J. Phys. A: Math. Gen. **27**, 8059 (1994).
[12] B. Li and M. Robnik, J. Phys. A: Math. Gen. **27**, 5509 (1994).
[13] B. Li and M. Robnik, J. Phys. A: Math. Gen. **28**, 2799 (1995).
[14] B. Li and M. Robnik, J. Phys. A: Math. Gen. **28**, 4843 (1995).
[15] T. Prosen, J. Phys. A: Math. Gen. **28**, L349 (1995).
[16] T. Prosen and M. Robnik, J. Phys. A: Math. Gen. **32**, 1863 (1999).
[17] G. Veble, M. Robnik, and J. Liu, J. Phys. A: Math. Gen. **32**, 6423 (1999).
[18] B. Batistić and M. Robnik, J. Phys. A: Math. Theor. **43**, 215101 (2010).
[19] S. Tomsovic and D. Ullmo, Phys. Rev. E **50**, 145 (1994).
[20] M. Martinez, O. Giraud, D. Ullmo, J. Billy, D. Guéry-Odelin, B. Georgeot, and G. Lemarié, Phys. Rev. Lett. **126**, 174102 (2021).
[21] M. Robnik, Eur. Phys. J.: Spec. Top. **225**, 959 (2016).
[22] M. Robnik, Nonlin. Phenom. Complex Syst. (Minsk) **23**, 172 (2020).
[23] E. J. Heller and S. Tomsovic, Phys. Today **46**, 38 (1993).

[24] V. Lopac, I. Mrkonjic, and D. Radic, Phys. Rev. E **59**, 303 (1999).
[25] V. Lopac, I. Mrkonjic, and D. Radic, Phys. Rev. E **64**, 016214 (2001).
[26] H. Makino, T. Harayama, and Y. Aizawa, Phys. Rev. E **63**, 056203 (2001).
[27] J. Chen, L. Mohr, H.-K. Zhang, and P. Zhang, Chaos **23**, 043137 (2013).
[28] L. A. Bunimovich, H.-K. Zhang, and P. Zhang, Commun. Math. Phys **341**, 3781 (2015).
[29] L. A. Bunimovich, G. Casati, T. Prosen, and G. Vidmar, Exptl. Math. **1**, 10 (2019).
[30] Č. Lozej, Phys. Rev. E **101**, 052204 (2020).
[31] H. Makino, PTEP **2022**, 093A02 (2022).
[32] Č. Lozej, D. Lukman, and M. Robnik, Phys. Rev. E **103**, 012204 (2021).
[33] Č. Lozej, D. Lukman, and M. Robnik, Nonlin. Phenom. Complex Syst. (Minsk) **24**, 1 (2021).
[34] Č. Lozej, D. Lukman, and M. Robnik, Physics **3**, 888 (2021).
[35] G. Contopoulos and M. Harsoula, Intl. J. Bifurcat. Chaos **20**, 2005 (2010).
[36] L. A. Bunimovich and L. V. Vela-Arevalo, Chaos: Interdisc. J. Nonlin. Sci. **22**, 026103 (2012).
[37] J. Tualle and A. Voros, Chaos Solitons Fractals **5**, 1085 (1995).
[38] A. Bäcker, S. Fürstberger, and R. Schubert, Phys. Rev. E **70**, 036204 (2004).
[39] M. V. Berry, Eur. J. Phys. **2**, 91 (1981).
[40] Č. Lozej and M. Robnik, Phys. Rev. E **98**, 022220 (2018).
[41] H.-D. Meyer, J. Chem. Phys. **84**, 3147 (1986).
[42] F. Steiner in *Universität Hamburg 1994: Highlights of Research for the 75th Anniversary*, edited by R. Ansorge (Reimer, Hamburg, 1994), pp. 543.
[43] R. Aurich, J. Bolte, and F. Steiner, Phys. Rev. Lett. **73**, 1356 (1994).
[44] E. Vergini and M. Saraceno, Phys. Rev. E **52**, 2204 (1995).
[45] Č. Lozej, Ph.D. thesis, University of Maribor; https://dk.um.si/IzpisGradiva.php?id=78037&langeng (2020) .
[46] Č. Lozej, B. Batistić, and D. Lukman, Quantum billiards, https://github.com/clozej/quantum-billiards/tree/crt_public (unpublished).
[47] B. Batistić and M. Robnik, J. Phys. A: Math. Theor. **46**, 315102 (2013).
[48] B. Batistić, Č. Lozej, and M. Robnik, Nonlin. Phenom. Complex Syst. (Minsk) **21**, 225 (2018).
[49] B. Batistić, Č. Lozej, and M. Robnik, Phys. Rev. E **100**, 062208 (2019).
[50] B. Batistić, Č. Lozej, and M. Robnik, Nonlin. Phenom. Complex Syst. (Minsk) **23**, 17 (2020).
[51] K. Husimi, Proc. Phys. Math. Soc. Jpn. **22**, 264 (1940).
[52] E. Wigner, Phys. Rev. **40**, 749 (1932).
[53] G. Vidmar, H.-J. Stöckmann, M. Robnik, U. Kuhl, R. Höhmann, and S. Grossmann, J. Phys. A: Math. Theor. **40**, 13883 (2007).
[54] B. Batistić and M. Robnik, Phys. Rev. E **88**, 052913 (2013).
[55] A. Wehrl, Rev. Mod. Phys. **50**, 221 (1978).
[56] D. Villaseñor, S. Pilatowsky-Cameo, M. A. Bastarrachea-Magnani, S. Lerma-Hernández, and J. G. Hirsch, Phys. Rev. E **103**, 052214 (2021).
[57] S. Pilatowsky-Cameo, D. Villaseñor, M. A. Bastarrachea-Magnani, S. Lerma-Hernández, and J. G. Hirsch, Phys. Rev. E **105**, 064209 (2022).
[58] S. Pilatowsky-Cameo, D. Villaseñor, M. A. Bastarrachea-Magnani, S. Lerma-Hernández, L. F. Santos, and J. G. Hirsch, Quantum **6**, 644 (2022).
[59] T. Prosen, Physica D **91**, 244 (1996).
[60] M. Kus, J. Mostowski, and F. Haake, J. Phys. A: Math. Gen. **21**, L1073 (1988).
[61] K. R. Jones, J. Phys. A: Math. Gen. **23**, L1247 (1990).
[62] S. Gnutzmann and K. Zyczkowski, J. Phys. A: Math. Gen. **34**, 10123 (2001).
[63] S. Pilatowsky-Cameo, D. Villaseñor, M. A. Bastarrachea-Magnani, S. Lerma-Hernández, L. F. Santos, and J. G. Hirsch, Nat. Commun. **12**, 1 (2021).
[64] Č. Lozej, G. Casati, and T. Prosen, Phys. Rev. Res. **4**, 013138 (2022).
[65] A. Bäcker, M. Haque, and I. M. Khaymovich, Phys. Rev. E **100**, 032117 (2019).
[66] N. Macé, F. Alet, and N. Laflorencie, Phys. Rev. Lett. **123**, 180601 (2019).
[67] G. De Tomasi and I. M. Khaymovich, Phys. Rev. Lett. **124**, 200602 (2020).
[68] L. Pausch, E. G. Carnio, A. Rodríguez, and A. Buchleitner, Phys. Rev. Lett. **126**, 150601 (2021).
[69] L. Pausch, E. G. Carnio, A. Buchleitner, and A. Rodríguez, New J. Phys. **23**, 123036 (2021).
[70] M. T. Eiles, A. Eisfeld, and J. M. Rost, arXiv:2111.10345.
[71] M. Serbyn, D. A. Abanin, and Z. Papić, Nat. Phys. **17**, 675 (2021).
[72] I. Ulčakar and L. Vidmar, Phys. Rev. E **106**, 034118 (2022).
[73] Q. Wang and M. Robnik, Phys. Rev. E **102**, 032212 (2020).
[74] Q. Wang and M. Robnik, Entropy **23**, 1347 (2021).
[75] G. Nakerst and M. Haque, arXiv:2203.09953.
[76] M. Robnik, J. Dobnikar, A. Rapisarda, T. Prosen, and M. Petkovsek, J. Phys. A: Math. Gen. **30**, L803 (1997).